



Computer Simulations for the PoGOLite Pathfinder Experiment

SEAN NICHOLAS BARKAS

Master's Thesis
Supervisor: Felix Ryde

TRITA-FYS 2010:23

Abstract

The Polarized Gamma-ray Observer (PoGOLite) is a balloon-borne instrument for measuring the polarization of soft gamma-rays/hard X-rays from celestial sources in the 25-80 keV energy range. Its pathfinder flight is scheduled to take place in August 2010 with a six hour observation of the Crab nebula and pulsar.

In this thesis, enhancements are made to the simulation software that is used to aid in the planning of the pathfinder experiment and analyse the data that will be gathered. These improvements facilitate studies of potential influences on PoGOLite's observations, including the effect of the detector's inclination angle on neutron background event rates, errors in how accurately the detector is pointed at its target, and failures of a photomultiplier tube (PMT) or the electronics it is wired to (FADC). It is found that detector inclination has no significant impact on background event rates, a 1° pointing error increases the minimum detectable polarization (MDP) for a six hour observation from $8.52 \pm 0.19\%$ to $13.7 \pm 0.5\%$, and loss of a hardware component can increase MDP insignificantly to $8.67 \pm 0.20\%$ for a failed PMT or $9.49 \pm 0.22\%$ for a failed FADC.

Additionally, a polarization dataset is built based on simulated data. This will be used to determine polarization degree and angle of observed photons.

Contents

Contents	iv
1 Introduction to PoGOLite	1
1.1 Polarization	1
1.2 Astronomical targets	2
1.2.1 Pulsars	2
1.3 PoGOLite	3
1.3.1 Polarimeter	4
1.3.2 Neutron background	5
1.4 Pathfinder flight	6
2 Computer simulations	7
2.1 Simulation software	7
2.2 Enhancements to polaripogo software	8
2.2.1 Polarization	8
2.2.2 Number of particles to simulate	9
2.2.3 Detector orientation	9
2.2.4 Upper and lower hemispheric neutrons	11
3 Analysis of simulated results	15
3.1 Determining valid events and scattering angles	15
3.1.1 Energy thresholds and adjustments	15
3.1.2 Scattering angle	17
3.1.3 Statistical uncertainty in event counts	18
3.2 Modulation and minimum detectable polarization	18
3.3 Influences on measurements	21
3.3.1 Neutron background	21
3.3.2 Pointing errors	21
3.3.3 Potential hardware failure	25
3.4 Polarization dataset	28
4 Conclusions and future work	31
4.1 Future work	32

A Using polaripogo software	33
A.1 Building	33
A.2 Running simulations	33
A.3 Analysis	34
A.4 History	35
List of Figures	36
List of Tables	37
Bibliography	39

Chapter 1

Introduction to PoGOLite

Astronomers have been studying celestial X-ray and gamma-ray sources since the 1960s, measuring their spectra, time variabilities, and projected images [9]. Observing at this portion of the electromagnetic spectrum presents a significant challenge because the Earth's atmosphere is opaque to such high energies, unlike radio or visible light radiation. X- and gamma-ray detectors must be placed into orbit or the upper atmosphere by rockets or balloons. Despite this challenge, satellite and balloon based experiments over the past few decades have provided a great deal of data about X-ray and gamma-ray sources. However, there is still little known about the polarization of the radiation coming from these high energy emitters.

1.1 Polarization

When light travels through space, the electric field is orthogonal to the direction of propagation. If the electric field oscillates in a straight line, the light is said to be linearly polarized. If the end of the field vector travels in a circle or ellipse, the light has circular or elliptical polarization, respectively [12].

There are two parameters used to describe linear polarization: angle and degree. The polarization *angle* describes the direction in which the electric field oscillates. Every photon in a beam of light does not necessarily oscillate in this same direction, though. Light is said to be unpolarized if each photon's electric field oscillates in a random direction. The percentage of light coming from a source that is polarized at a given angle is the *degree* of polarization, while the remaining proportion is unpolarized.

Three processes which produce polarized light are synchrotron emission, curvature radiation, and inverse Compton scattering [2]. *Synchrotron radiation* is produced when electrons moving at relativistic velocities spiral along magnetic field lines. Radiation is emitted in the direction of motion, and is linearly polarized in the plane of the electrons' circular motion. If the motion of the electrons along the field lines is more dominant than the circular motion, the emission process is instead called *curvature radiation*. In this case, the radiation emitted is strongly

polarized in the plane of the curving magnetic field [4]. Finally, in *inverse Compton scattering*, a photon scatters off a relativistic electron, gaining energy in the process. Even relatively low energy photons can be boosted to gamma-ray energies via inverse Compton scattering.

1.2 Astronomical targets

Polarization of X-ray and gamma-ray astronomical sources, such as pulsars and accreting black holes, can provide information about their geometry, magnetic fields, and radiation mechanisms [7]. The primary target of the PoGOLite pathfinder flight will be the Crab Nebula and the pulsar within.

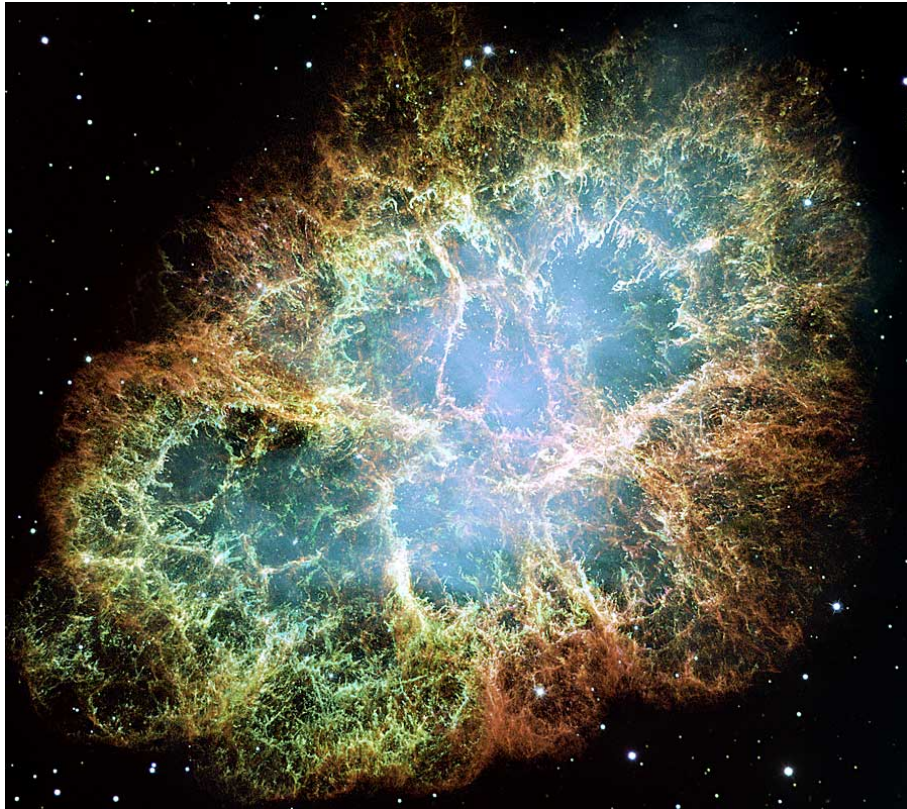


Figure 1.1: Crab Nebula viewed from the Hubble Space Telescope. <http://antwrp.gsfc.nasa.gov/apod/ap091025.html>

1.2.1 Pulsars

Pulsars are rotating neutron stars, which themselves are highly dense remnants of approximately 1.5-5 solar mass stars that have destroyed themselves in a supernova. Neutron stars are not capable of producing radiation through nuclear fusion

in the manner of normal stars. The angular momentum and strong magnetic field of the progenitor star are retained by the neutron star remaining after the explosion. Neutron stars rotate extremely rapidly compared to their much larger, slower rotating progenitors due to conservation of angular momentum. If the magnetic field and the rotation axis are not aligned, a powerful, pulsed beam of radiation is generated. Originally pulsars were detected by rapid, regular flashes in the radio wave spectrum, but they also emit at gamma-ray and other frequencies.

The precise way in which the energetic beam observed from pulsars is produced is not yet completely known. Three primary models have been proposed: polar cap, outer gap, and caustic [2]. In the *polar gap* model, electrons and positrons are accelerated near the magnetic poles of the neutron star, emitting curvature radiation. This radiation also interacts with the magnetic field, producing more electrons and positrons. These in turn emit synchrotron radiation, and a cascade of synchrotron and curvature emitted gamma-rays can be observed. In the *outer gap* model, particles are accelerated in the vacuum gaps in the outer portion of the neutron star's magnetosphere. These particles emit curvature radiation and cause inverse Compton scattering, producing secondary positron and electron pairs which cause more inverse Compton scattering and emit synchrotron radiation. The *caustic model* is a combination of the other two. In it, radiation may be produced in a region extending from the polar cap along the surface of the last open magnetic field line.

Recent observations have essentially eliminated the polar cap model, but the outer gap and caustic models still fit existing data well. The polarization properties of the observed gamma-rays emitted by all three models differ, though. It is hoped that polarization data collected by PoGOLite will help demonstrate the validity of either the outer gap or caustic models.

1.3 PoGOLite

Figure 1.2 shows the main components of PoGOLite's polarimeter. Photons from its target enter through the slow plastic scintillators. The interaction of these photons with the material in the fast plastic scintillators produces visible light that will be measured by a photomultiplier tube (PMT) attached below. Bismuth Germanium Oxide (BGO) crystals make up the side anti-coincidence shields (SAS) as well as bottom anti-coincidence shield. These shields are used to detect background particles, such as atmospheric neutrons, that could cause false events to be recorded in the fast scintillators. Each tube consisting of a fast and slow plastic scintillator with its bottom BGO crystal is referred to as a phoswich detector cell (PDC). The full version of PoGOLite will have 217 PDCs, but the pathfinder version that is focused on in this thesis has 61.

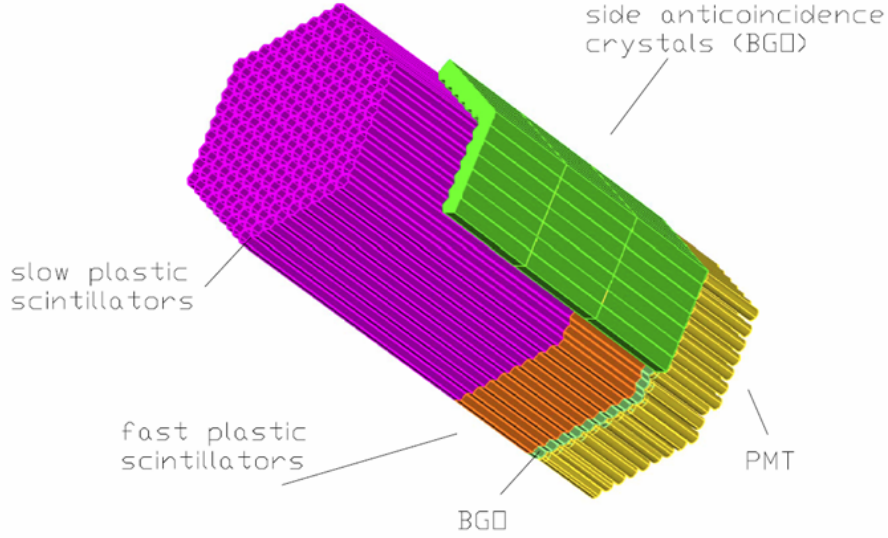


Figure 1.2: Components of the PoGOLite polarimeter, 217 PDC version. Some of the side anti-coincidence shield has been cut away to show the fast and slow scintillators and bottom BGO crystals. From [2].

1.3.1 Polarimeter

Polarization of incoming photons will be measured through the processes of Compton scattering and photo absorption [15]. Compton scattering occurs when highly energetic photons hit an electron, and some of the incident photon's energy is transferred to the electron. The rest is emitted in a lower energy photon that scatters off in another direction. This scattered photon is likely to travel on a path orthogonal to the incident photon's polarization vector with a probability given by the Klein-Nishina formula,

$$\frac{d\sigma}{d\Omega} = \frac{1}{2} r_e^2 \frac{k^2}{k_0^2} \left(\frac{k}{k_0} + \frac{k_0}{k} - 2 \sin^2 \theta \cos^2 \phi \right), \quad (1.1)$$

where r_e is the classical electron radius, k_0 is the momentum of the incident photon, and k is the momentum of the scattered photon. ϕ and θ are the azimuthal and polar scattering angles, respectively. The scattered photon can be measured in another fast scintillator nearly simultaneously with the Compton scattering event in the first. Calculating the angle between the PMTs which register the two events provides the scattering angle, from which the polarization angle of the incident photon can be deduced by adding or subtracting 90° .

Incoming photons from sources outside the instrument's field of view will hit the walls of the hollow slow scintillators before reaching the fast scintillators. The PMTs will measure these slow hits, but the scintillation decay time in the slow scintillators

is much greater than in the fast scintillators, so any event with the slower decay time measured can be vetoed.

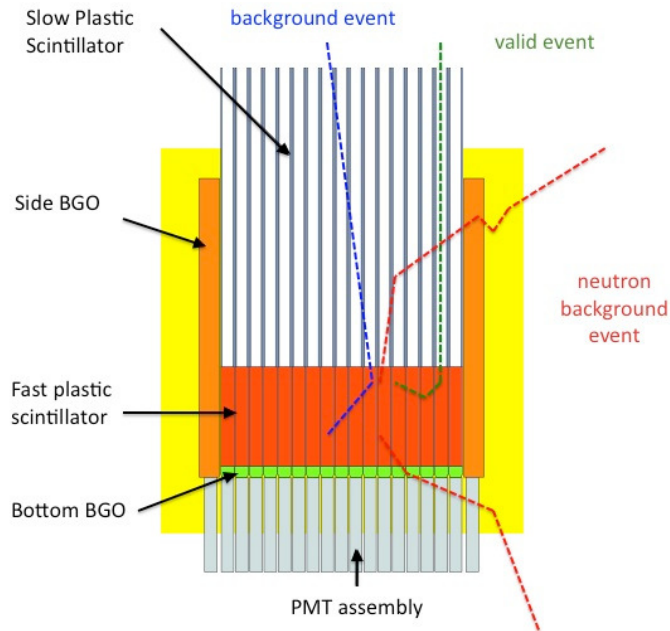


Figure 1.3: Valid and background events measured by PoGOLite. The blue particle coming in through the top can be vetoed because it hits the wall of a slow scintillator. The neutron events from the side and bottom will be vetoed since they collide with the BGO shield. The green particle coming straight in through the top will be counted as a valid event. From [2].

1.3.2 Neutron background

In addition to photons from non-target sources that hit the slow scintillators, other background particles may also add noise to PoGOLite's observations. Cosmic rays and atmospheric protons that pass through the detector from all sides can trigger false events, but atmospheric neutrons are the most significant background that must be filtered out [14]. Neutrons entering from the bottom of the detector will hit the BGO crystals between the PMTs and fast scintillators. These crystals, like the slow scintillators, have a longer decay time than the fast scintillators, so these events can be vetoed in the same way. Additionally, neutrons entering from the sides will hit the SAS BGO crystals. These are attached to PMTs like those connected to the PDCs, and any hits measured here can be also used to veto simultaneous hits inside the detector.

To provide additional passive shielding to these anti-coincidence systems, the detector's pressure chamber will be covered in a layer of polyethylene. The design

of this neutron shield's shape has been optimized via computer simulations in [19].

1.4 Pathfinder flight

The pathfinder flight of PoGOLite will take place in August 2010 with a launch from Esrange in northern Sweden. The main goal of this flight is to test the detection method and actual detector hardware. Six hours of observation time during this flight are planned, with the primary target being the Crab. The possibility for a longer flight is possible, though, if conditions allow. In this case it may also be possible to spend some time observing radiation caused by the accretion of matter onto the black hole Cygnus X-1. Future experiments with PoGOLite are planned to both have longer duration and use the larger, 217 PDC polarimeter.

Chapter 2

Computer simulations

Computer simulations have been important throughout the development of PoGO-Lite. It is cheaper and faster to run a simulation to test out new hardware designs or detector responses to different types of incoming particles than building a prototype and running beam test experiments. The simulation software used to predict what is expected to be measured by PoGO-Lite, and later assist in the analysis of observational data, is introduced in this chapter. This is followed by a description of enhancements I have made to this software, most of which allow users to set a number of parameters for different simulations that they may wish to do. Explanations of why one would want to adjust these parameters and other motivations for the changes made are given as well.

2.1 Simulation software

Our simulation software, named polaripogo, is built around the Geant4 toolkit [8]. Geant4 provides a framework written in C++ for building software that accurately simulates particles passing through matter.

Geant4 version 9.2.p01 is used for the simulations in this thesis, along with CLHEP 2.0.4.2 [16] and data files G4ABLA 3.0, G4EMLOW 6.2, G4NDL 0.2, G4NDL 3.13, PhotonEvaporation 2.0, and RadioactiveDecay 3.2. These data files are also available from the Geant4 web site [8]. Problems have been found with the implementation of Rayleigh and Compton scattering in Geant4 [10], and a fix for this has not yet been integrated with the mainline Geant4 source code. I have therefore patched the Geant4 installation used for all of my simulations with a fix from T. Mizuno that corrects the behaviour of Compton and Rayleigh scattering [17].

Appendix A provides information on where to find the polaripogo software, along with usage instructions and its development history.



Figure 2.1: PoGOLite as rendered by the polaripogo simulation software. The grey enclosure is a polyethylene neutron shield discussed in [14, 19], the blue cylinder is the pressure chamber that houses the polarimeter, and the cyan hexagonal tubes are the PDCs.

2.2 Enhancements to polaripogo software

I have added a number of features to polaripogo throughout this thesis work. Most of these are parameters that we can adjust before a simulation run and see how measured results are affected. The parameters are generally provided to the program as command line arguments so that we may easily script several simulations to run in succession, each with one parameter changed slightly from the previous run.

2.2.1 Polarization

One of the first new features I implemented was a way to control the polarization angle of the photons in the simulation. Previously this could only be changed by hard-coding a vector giving the angle into the source code and recompiling. Now it is possible to simply give a command line argument when starting a simulation that sets each photon to be polarized at this angle, which makes running simulations of several different polarization angles substantially easier.

I also made it possible to specify the degree of polarization, where a percentage of the photons in the simulation equal to the degree are polarized at the desired

angle and the rest are unpolarized. This option was later removed, though, because it is easy to instead combine output from simulations of unpolarized and 100% polarized photons during analysis to approximate any desired degree of polarization. For example, if we want to look at data where the photons are polarized at some angle α and degree d (see section 1.1), we can take d percent of the events from a simulation where all photons are 100% polarized at angle α and $100 - d$ percent of the events from a simulation with only unpolarized photons. This allows us to run a single simulation covering the desired observation time with unpolarized photons, and one simulation for each polarization angle we wish to look at, i.e. (number of polarization angles) + 1, instead of needing to run (number of polarization angles) \times (number of polarization degrees) simulations.

A major reason to simulate polarization degree and angle is to build an array of simulation outputs for all possible degrees and angles of polarization we could potentially see from PoGOLite’s observations of the Crab nebula and pulsar. This dataset will be compared with real observational data after the PoGOLite pathfinder flight in order to identify the polarization properties of the Crab. See section 3.4 for details on how observational data may be analysed by comparison with this dataset.

2.2.2 Number of particles to simulate

The next feature I implemented was a way to specify the duration of a simulated observation and use that to automatically compute the number of photons or other particles to bombard the detector with. Prior to this addition, it was necessary to specify the number of particles or photons explicitly before running a simulation. Calculating this number in the software, based on the flux from a particle source and the source’s area, makes running simulations more convenient.

polaripogo contains a number of C++ classes that represent various cosmic ray models we might want to simulate. In this thesis we use only two—CrGammaCrab for soft gamma rays in the range 10-200 keV and CrNeutron for atmospheric neutrons that are our primary source of background noise. Each of these cosmic ray model classes has a function that will return the energy integrated flux of this type of particle or photon in units [count/s m² sr]. I added code that calls this function and multiplies the result by the duration of the observation that the user has specified, the area of the simulated disc from which particles originate (see section 2.2.3), and the solid angle returned by the cosmic ray model’s `solidAngle()` function. We are then left with the number of particles that must be generated during the simulation.

2.2.3 Detector orientation

Polaripogo places a model of PoGOLite pointing straight up in the simulation world. The starting position of each simulated particle is chosen as a vector going from the centre of the detector in a direction dependent on the cosmic ray model in use to somewhere on a sphere surrounding the instrument. The initial direction of travel

for the particle is then a vector pointing in the opposite direction to this position vector. For photons from the Crab, every photon starts directly above the detector and is shot straight down into it. The starting position of neutrons, however, can be anywhere on the imagined sphere surrounding PoGOLite. These starting positions for particles are then adjusted to be randomly placed on a disc with diameter

$$d = \sqrt{l^2 + w^2 + h^2},$$

where $l = w$ is the diameter of the detector, and h is its height. The direction the particles move in is not changed, however—it is orthogonal to this disc. The size of the disc ensures that it always completely covers the detector no matter where it may be placed in the space surrounding it. Figure 2.2a shows this disc and a number of trajectories for simulated photons from the Crab when the detector is pointing straight at it.

I added code to polaripogo that allows us to simulate changes in the angle of inclination of the detector. This does not actually change the orientation of the detector within the simulation world, though. Instead we rotate the starting position and direction of the particles. As an example, figure 2.2b shows how we simulate the detector pointing at something 10 degrees away from the Crab. Being able to specify this inclination angle will be useful in measuring how our measurements may be affected by errors in pointing the detector at its target.

Adjusting the inclination angle will also be useful for simulating neutron background. The inclination or elevation angle of the detector will change throughout the flight to track its target, and a greater percentage of the background neutrons come from the atmosphere below PoGOLite than above it (see section 2.2.4). The portions of the detector pointing downward towards the Earth and hence being exposed to higher neutron flux will therefore also change throughout the flight. The angle and location at which neutrons hit the detector affect how likely a false event will be registered due to differences in the thickness of the neutron shielding and the internal geometry of the detector, so it is important that we simulate the neutron background for all orientations PoGOLite is expected to have throughout our observations.

A related change I made to the software allows us to simulate random small changes to the direction the detector points for each particle that is generated. Wind fluctuations, vibrations, and small adjustments from the instrument’s attitude control system will perturb the direction the detector points away from its target continuously throughout the flight. These perturbations are accounted for by adjusting the inclination angle of each particle by a random amount chosen according to a Gaussian distribution that has a standard deviation specified by the user.

Finally, I also added an option to polaripogo which lets the user adjust the rotation of the detector about its lengthwise axis. This will allow us to measure any systematic bias of the detector by duplicating simulations for different rotation angles and seeing how measurements of polarization angle are affected. During

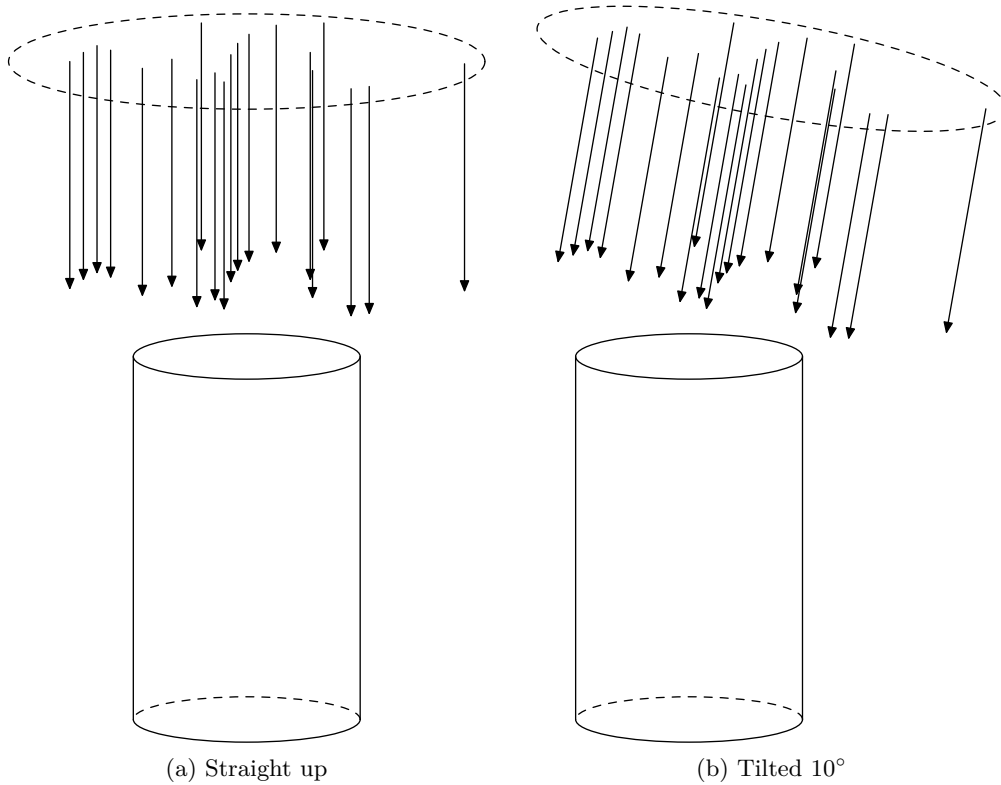


Figure 2.2: Arrangement of detector and incoming photons for simulating aiming directly at the Crab (a) and with inclination angle 10° off from pointing directly at the target (b). The vectors represent photon trajectories, only some of which will hit the detector, and the dashed ellipses above the detectors show the area from which photons may originate.

actual flights of PoGOLite, the detector will be rotated continuously to minimize any systematic errors that might exist.

2.2.4 Upper and lower hemispheric neutrons

In the version of the polaripogo code I started with, there were two models for simulating neutron backgrounds—one with all neutrons coming from a hemisphere below PoGOLite, and the other with incoming neutrons coming with equal probability from all directions. The reason for this is that we expect a greater number of neutrons to be coming from the thicker atmosphere below the detector than the number of neutrons coming from above. This property could be accounted for by combining a run with isotropic neutrons and an additional simulation run with just the lower hemisphere model [19]. In [1] it was shown that at a magnetic latitude of 42° N and atmospheric depth 5 g/cm^2 , which corresponds to an altitude of 36 km

[14], roughly 80% of of neutrons in the energy range 10-100 MeV would be moving upwards. While this altitude is close to that at which PoGOLite will fly, our simulations will be accounting for a wider energy range for neutrons, from 1 keV to 1 GeV. Additionally, the latitude for the pathfinder flight from Kiruna, Sweden will be much higher than 42° , and we expect that characteristics of neutrons at this latitude to be different [22]. However, we shall continue to assume that the upward moving, lower hemispheric neutrons will account for 80% of the total neutron flux in our simulations.

I have replaced the lower hemispheric and isotropic neutron models with a single model that generates neutrons from the lower hemisphere 80% of the time. Each cosmic ray model in polaripogo has a function `dir()` that is called to determine what direction in spherical coordinates the particle will come from. It returns a pair of angles, inclination and azimuth. We shall call the inclination angle θ , the azimuth angle ϕ , and use a function `rand(a, b)` to generate a uniform random number in the interval (a, b) . Figure 2.3 shows this spherical coordinate system.

If one wishes to pick the direction to be a random point on a sphere, such as is done in the old model with isotropic neutrons, `dir()` picks the azimuth angle to be any possible random direction,

$$\phi = \text{rand}(0, 2\pi). \quad (2.1)$$

The inclination angle is in the range $0 \leq \theta \leq \pi$ in the isotropic model, but to avoid bunching points near the poles of the sphere [24], we cannot pick θ according to a uniform random distribution. Instead `dir()` returned inclination

$$\theta = \arccos(\text{rand}(-1, 1)) \quad (2.2)$$

in the isotropic neutron model and

$$\theta = \arccos(\text{rand}(-1, 0)) \quad (2.3)$$

in the lower hemisphere neutrons model. The determination of azimuthal angle is unchanged in the lower hemisphere model.

In my new model where 80% of the neutrons come from below, `dir()` now computes the inclination in the following way:

$$\begin{aligned} x &= \text{rand}(-4, 1) \\ \theta &= \begin{cases} \arccos(x/4) & \text{if } x < 0 \\ \arccos(x) & \text{otherwise.} \end{cases} \end{aligned} \quad (2.4)$$

Azimuthal angle is again computed with (2.1). Figure 2.4 shows an example of how the inclination angles are distributed with the previous two models for isotropic and lower hemispheric only neutrons as well as my new model with 80% coming from below.

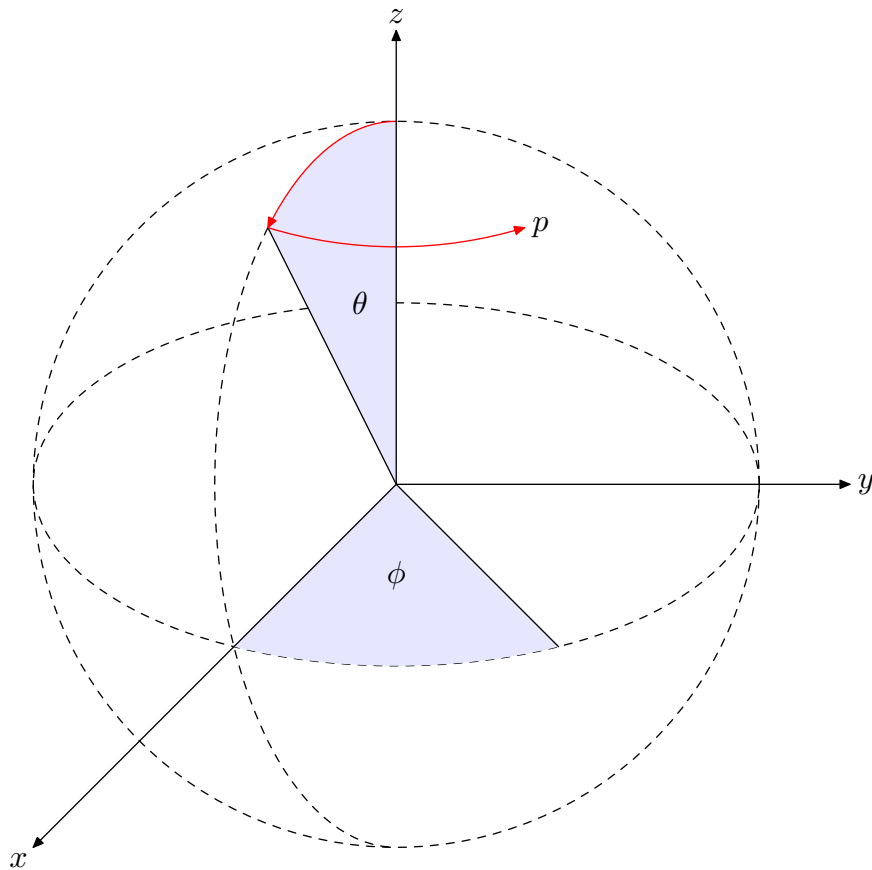


Figure 2.3: Coordinate system for picking direction of incoming particles. A particle at point p is picked by starting at the zenith (the point where the positive z axis intersects the sphere outlined with dashed lines) and first rotating across the surface of the sphere by inclination angle θ about the y axis, then rotating by azimuth angle ϕ about the z axis. The detector, not shown, has its centre at the origin and points towards zenith.

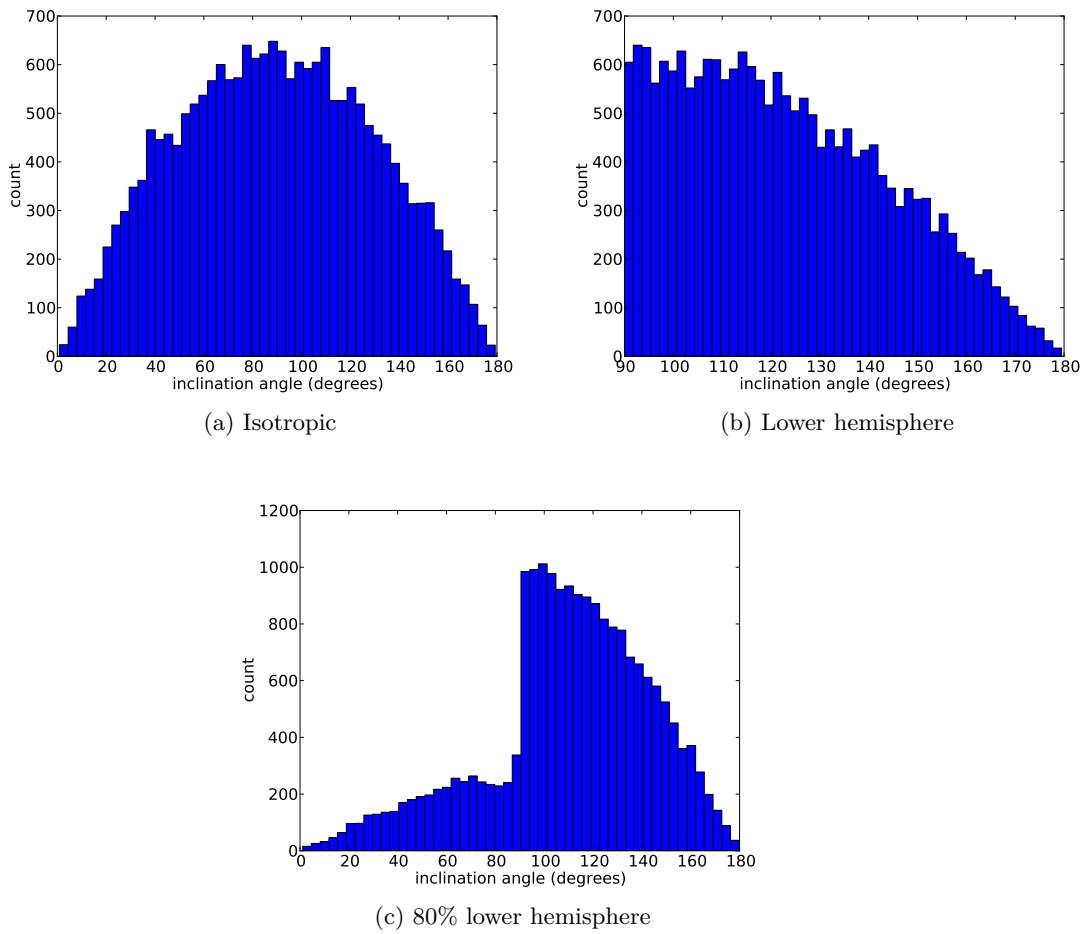


Figure 2.4: Distribution of inclination angle (θ) component of neutron direction for 20,000 random neutrons using the two initial polaripogo neutron cosmic ray models (top) and my new unified model (bottom)

Chapter 3

Analysis of simulated results

This chapter begins with a discussion on the steps taken to process raw simulation data generated by polaripogo into a list of valid events—simultaneous energy depositions in fast scintillators and the angle between those hit locations. Next, the minimum detectable polarization (MDP) degree is discussed. This is followed by a description of a number of possible sources of errors in the measurements made and their effects on the MDP. Finally, a description of a possible procedure for determining the polarization angle and degree from a real observation of PoGOLite by comparing with an array of simulated data is given.

3.1 Determining valid events and scattering angles

A polaripogo simulation produces an output file with a list of events, each corresponding to a single particle fired at PoGOLite that resulted in at least one “hit” somewhere in the detector. For each of these events, polaripogo saves the primary particle’s type, mass, and momentum. Additionally a list of all the detectors where hits were registered are saved with the energy deposited therein and the type of particle. This particle in many cases is different from the primary particle due to various physical processes that take place during particle collisions. Given this output file from polaripogo, we run it through a script (see appendix A.3) that picks out valid events and for each of those events measures the azimuth scattering angle of photons deposited in the simulated PoGOLite’s fast scintillators. This event extracting script is based on a collection of Python [23] and ROOT [3] scripts by Tsunefumi Mizuno [17] and Kristoffer Myrsten [19], but was rewritten by me during this thesis work in an attempt to make the process of analysing polaripogo simulation output easier.

3.1.1 Energy thresholds and adjustments

Hadronic particles that interact with the detector will have a lower light yield than photons with equivalent energy [19]. Therefore any particles found in the detector

which came from primary neutrons or other hadrons have their energy quenched according to data from [11]. Table 3.1 shows the quenching functions applied to the energy for particles in the fast or slow scintillators. All types of particles in either the bottom or side anti-coincidence BGO detectors are quenched by having their energy divided by 10. Photons, electrons, and positrons found in any detector are excluded from this quenching.

Table 3.1: Quenching of particles deposited in fast and slow scintillators resulting from a primary neutron. Protons and α particles are quenched with quadratic functions at lower energies and linear functions at higher energies, ^{12}C is linearly quenched at all energies, and other particle types have their energies quenched to zero. Photons, electrons, and positrons are not quenched at all.

Scattered particle type and energy	Quenching function (energy E in keV)
proton < 1000 keV	$5.64 \times 10^{-2}E + 1.19 \times 10^{-4}E^2$
proton ≥ 1000 keV	$0.1754E$
$\alpha < 4000$ keV	$1.45 \times 10^{-2}E + 8.78 \times 10^{-6}E^2$
$\alpha \geq 4000$ keV	$0.0495E$
^{12}C	$6.2 \times 10^{-3}E$
others	0

The next step is to eliminate events that appear to not be caused by photons from the Crab. As discussed in section 1.3, some of PoGOLite's detectors are used to veto invalid events from incoming particles that did not come from the target it is pointed at. If more than 10 keV is deposited in the slow scintillators, or 30 keV in either the side anti-coincidence shields or bottom BGO scintillators, the event is skipped.

Each remaining event is then checked to see if there were any hits in the fast scintillators. If so, the PMT for the corresponding scintillator should measure the hit. However, the PMTs are not able to exactly measure the energy deposited, so the energy is randomized with a Poisson spread for energies lower than 20 keV, or a Gaussian spread at higher energies. The minimum energy threshold for a PMT is 2 keV, so any hits in a given fast scintillator with energy below this after randomization are discarded [5].

Additionally, an event will be skipped if there are less than two or more than three fast scintillators with hits. Only two fast hits are needed to measure an azimuthal scattering angle, but if there is a third event it is considered as well for the sake of calculating the total amount of energy deposited. This total energy across the two or three fast scintillators now is summed and if it is within the range of 25-80 keV the event is kept, and events with total energy outside this range are discarded.

3.1.2 Scattering angle

Now that all valid events have been picked out from the simulation output, the next step is to measure the angle between the fast scintillator hits. If there were three fast hits, the two with the highest energy are used for calculating this angle. For real observations with PoGOLite it will be impossible to know where precisely particles are within a detector, so the calculation of the angle between the two hits will be based on the spatial coordinates of the centres of the corresponding scintillators. Particles will of course not always happen to land exactly in the middle of the detectors, though, so two events with quite different scattering angles will often be measured to be the same simply because they took place in the same detectors. Figure 3.1 shows an example of this problem.

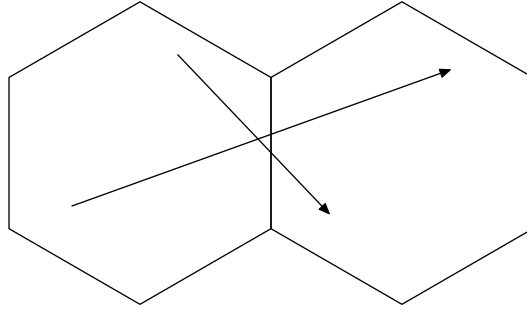


Figure 3.1: Example of two possible events in adjacent fast scintillators that will both be measured as having the same scattering angle: the angle between the scintillator centres.

In order to account for the range of possible scattering angles between two detector cells, the centre-to-centre angle is randomized according to a Gaussian distribution with experimentally determined

$$\sigma = 11.09 \left(\frac{1}{d + 0.356} + \frac{1}{d - 0.356} \right)^\circ, \quad (3.1)$$

where d is the distance between the detector centres in units of the fast scintillator width (2.775 cm) [18]. Figure 3.2 from [2] shows the errors created by failing to smear the measured scattering angles. The signal measured is 100% polarized at 0° . The green curve corresponding to smeared data shows maximums near $\pm 90^\circ$, which is expected for a signal polarized at 0° . The unsmeared data's red modulation curve is out of phase from this, so it would imply a different, incorrect polarization angle. Additionally, the unsmeared modulation curve has a significantly higher amplitude, suggesting a greater modulation factor. This data would therefore result in overestimation of the degree of polarization, too.

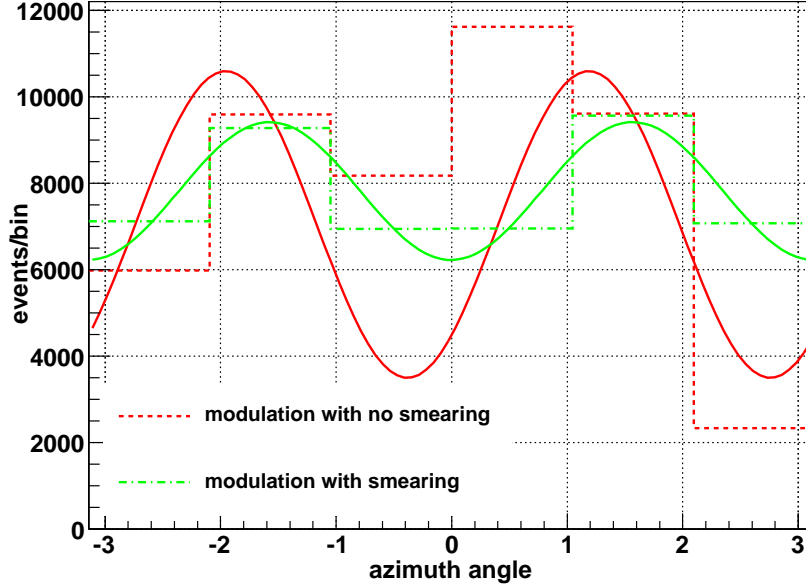


Figure 3.2: Distributions of scattering angles for a signal polarized 100% at 0° with (green curve) and without (red curve) smearing. Histograms are shown as dotted lines, and the solid lines show fits to modulation curves. From [2].

3.1.3 Statistical uncertainty in event counts

A degree of statistical uncertainty is expected in the number of events measured from a given simulation output file. Running `extract_events.py` (see A.3) 1000 times on the same one hour Crab simulation resulted in a distribution of event counts shown in figure 3.3. The Poisson distribution fits this histogram slightly better than the normal probability distribution function. It is also very convenient to calculate its standard deviation $\sigma = \sqrt{n}$ for n events, so this σ is used for the error bars on event counts in the sections below.

3.2 Modulation and minimum detectable polarization

The steps detailed above in section 3.1 provide a list of angles between fast scintillators inside a simulated PoGOLite. Each of these angles correspond to a quantity of energy measured in two fast scintillators simultaneously by their attached PMTs. Most of these events, it is hoped, are produced by gamma rays from PoGOLite’s target entering the detector and Compton scattering when they hit the fast scintillators, although many are false events produced by background particles such as atmospheric neutrons.

This collection of scattering angles can be plotted as a histogram such as those

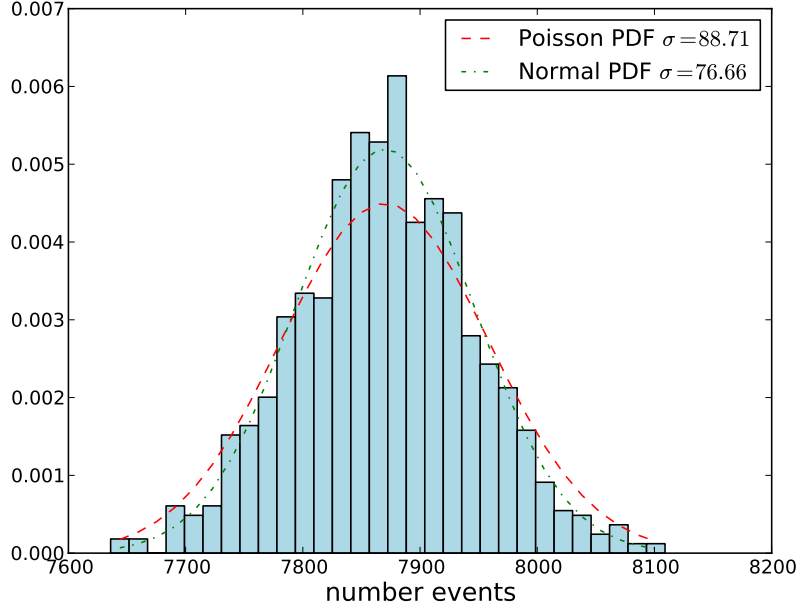


Figure 3.3: Distribution of event counts for 1000 runs of `extract_events.py` on the same one hour Crab simulation.

in figure 3.4. These histograms show that the unpolarized signals (3.4b and 3.4c) have a distribution of scattering angles that appears flatter than those that are polarized (3.4a and 3.4d).

We can fit a sine function to these histograms, and we call this the modulation curve. The modulation factor M is

$$M = \frac{c_{max} - c_{min}}{c_{max} + c_{min}}, \quad (3.2)$$

where c_{max} and c_{min} are the maximum and minimum number of events, respectively, of the modulation curve. A higher modulation factor corresponds to a higher degree of polarization in the signal.

The minimum detectable polarization, or MDP, is the lowest degree of polarization a polarimeter can accurately measure. According to [2], at a 99% confidence level the MDP is

$$MDP_{99\%} = \frac{4.29}{M_{100}R_S} \sqrt{\frac{(R_S + R_B)}{T}} \quad (3.3)$$

where M_{100} is the modulation factor of a 100% polarized source, R_S and R_B are the rates of source and background events per second, respectively, and T is the observation time in seconds.

In [2], M_{100} is calculated to be 0.278 ± 0.005 for a 100% polarized Crab source. Across 19 simulations of six hour Crab observations, the mean number of events

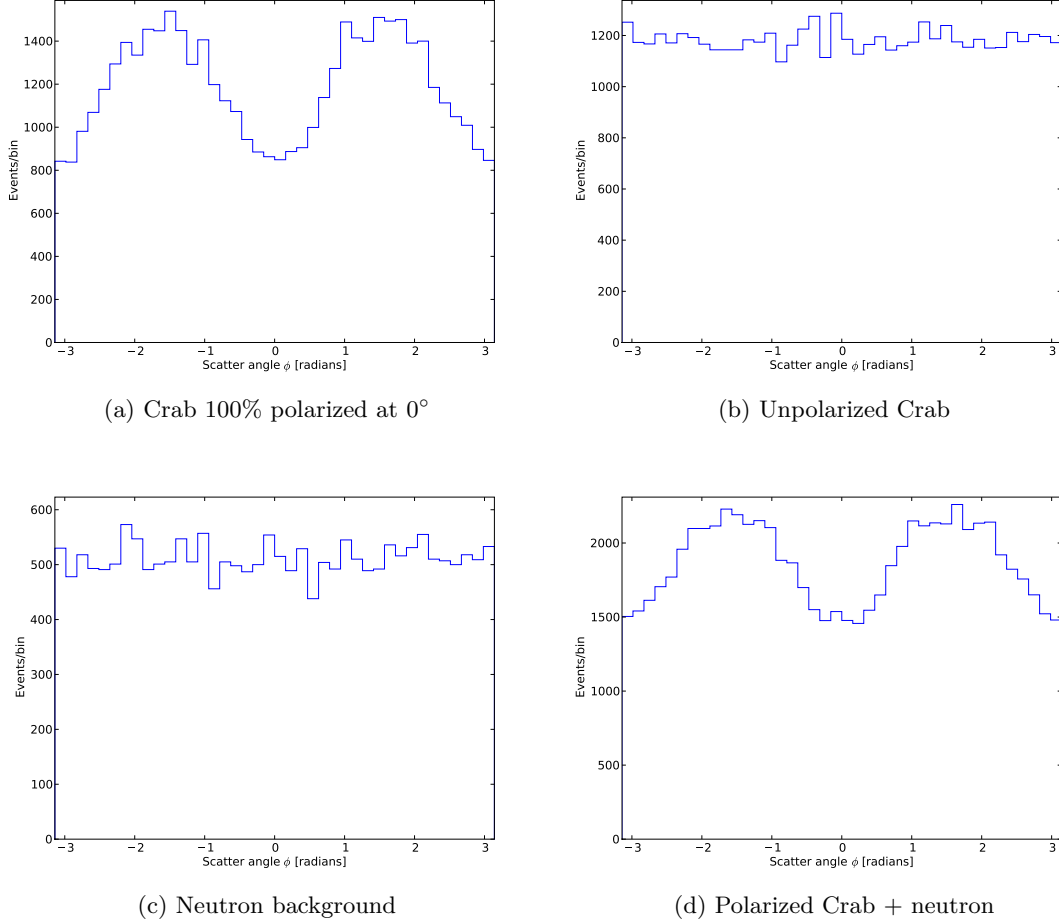


Figure 3.4: Distributions of azimuthal scattering angles for six hour simulations of Crab signals and neutron background.

measured was 47,160. Assuming a Poisson distribution on this count (see section 3.1.3), an error range of $\sqrt{47160} \approx 217$ is used. Dividing these by the length of the observation time gives the Crab signal rate

$$R_S = \frac{47160 \pm 217}{21600 \text{ s}} = 2.18 \pm 0.01 \text{ s}^{-1}. \quad (3.4)$$

We compute the background rate R_B based on the number of false events measured during six hours of neutron simulations, 20,455, the same way:

$$R_B = \frac{20455 \pm \sqrt{20455}}{21600 \text{ s}} = 0.947 \pm 0.007 \text{ s}^{-1}. \quad (3.5)$$

Putting these values for R_B , R_S , M_{100} and $T = 21,600 \text{ s}$ into (3.3) gives an MDP of $8.52 \pm 0.19\%$ for PoGOLite's planned six hour observation of the Crab.

3.3 Influences on measurements

There are several possible sources of error in the measurements that will be made by PoGOLite. The most significant error source are the false events triggered by background neutrons discussed in section 1.3.2. Also, many of the photons we wish to measure from the Crab will be absorbed by the atmosphere before reaching the detector, reducing the number of events we will be able to measure. The results included in this thesis assume a constant atmospheric depth of 5 g/cm^2 for determining the amount of atmospheric attenuation. But, the actual amount of atmosphere we must observe through will change substantially throughout the flight as the Crab's elevation angle above the horizon changes. A detailed discussion of this along with calculations of how the changing atmospheric depth attenuates photons we wish to measure from the Crab is given in [2].

Some additional possible error sources are considered below.

3.3.1 Neutron background

As discussed in section 2.2.4, simulations of background neutrons are done with 80% of the neutrons coming from below. However, the inclination angle of PoGOLite will change while tracking the Crab, as mentioned above, and therefore the portions of the instrument subjected to the higher neutron flux from the atmosphere below will also change throughout the experiment. According to [20, 2], the inclination angle of PoGOLite while tracking the Crab will vary from about $46 - 62^\circ$ during the flight—see figure 3.5.

I performed 12 simulations of neutron backgrounds for half an hour with the inclination angle corresponding to the Crab's inclination at that time interval. Figure 3.6 shows the total number of false events measured by PoGOLite for each of these inclination angles, plus three other angles (0° , 10° , and 20°). These smaller angles are included to show if there is any effects on the number of false events measured when pointing closer to zenith, even though the Crab will never be this far above the horizon during the pathfinder flight. Larger inclination angles than 62° are not considered, though, because atmospheric attenuation of photons from targets this close to the horizon would be too great.

There does not appear to be a significant correlation between the inclination angle of the detector and the number of background triggered false events measured. Therefore it should be reasonable to consider the rate of background events to be constant throughout the pathfinder experiment. For further discussion, see [2].

3.3.2 Pointing errors

Now we shall take a look at how pointing accuracy can affect observations. First, we do a few calculations that predict how tilting the detector ought to reduce the number of particles that can pass uninhibited through the slow scintillators.

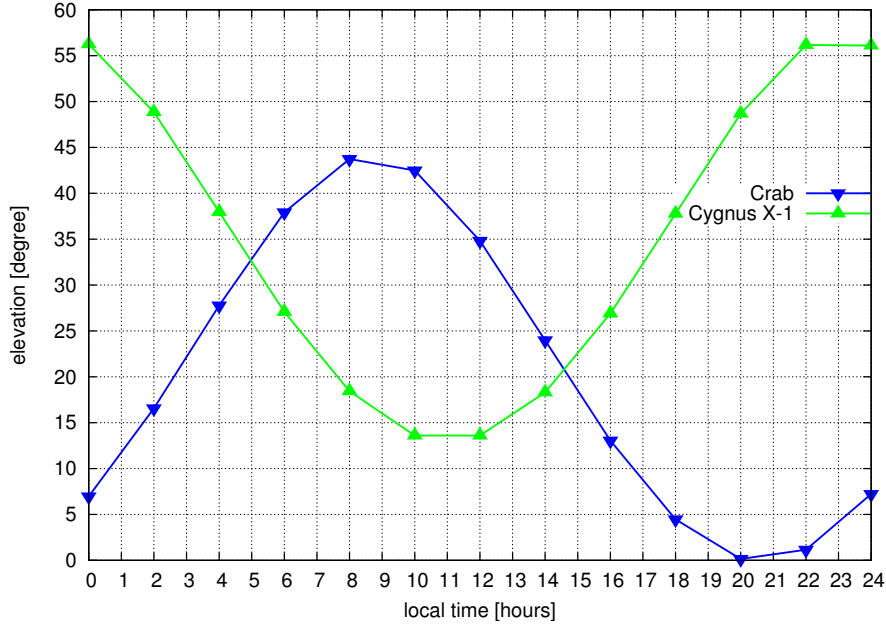


Figure 3.5: Elevation angle of targets during PoGOLite pathfinder flight (inclination angle is 90° - elevation). Observations of the Crab will begin upon reaching observation altitude at approximately four hours with an elevation angle of 28° , or inclination of 62° , and continue at least until hour ten. The smallest inclination angle during this time will be 46° at eight hours. From [2].

Assuming a constant flux of incoming particles, one can assume that for a given duration of observation the number of events registered by PoGOLite will be proportional to the area of the PDC openings which a particle can pass through the slow scintillator without hitting its walls. All of the PDCs are assumed to be the same and parallel to one another, so we will consider just a single PDC. Also, we approximate the PDC as a cylinder instead of using its true hexagonal shape so that the direction the detector is inclined doesn't matter, and to make area calculations simpler. Figure 3.7a shows a top down view of the two circular¹ end-points of our cylindrical approximation of a tilted slow scintillator. The shaded region in the middle, the intersection of these two circles, is the region through which particles can pass without hitting the scintillator walls. We shall call the area of this region A_t , and the area of each circle A_s ($A_s = A_t$ when the detector is pointing straight at its target). Similarly we will call the event count for the straight-on detector n_s and n_t for a tilted detector.

A_t can be computed knowing only the radius of the circle r and the distance

¹These two circles would actually look like ellipses if we looked down from the top of a tilted cylinder, but we are considering such small inclination angles that it makes little difference to use the more convenient circles.

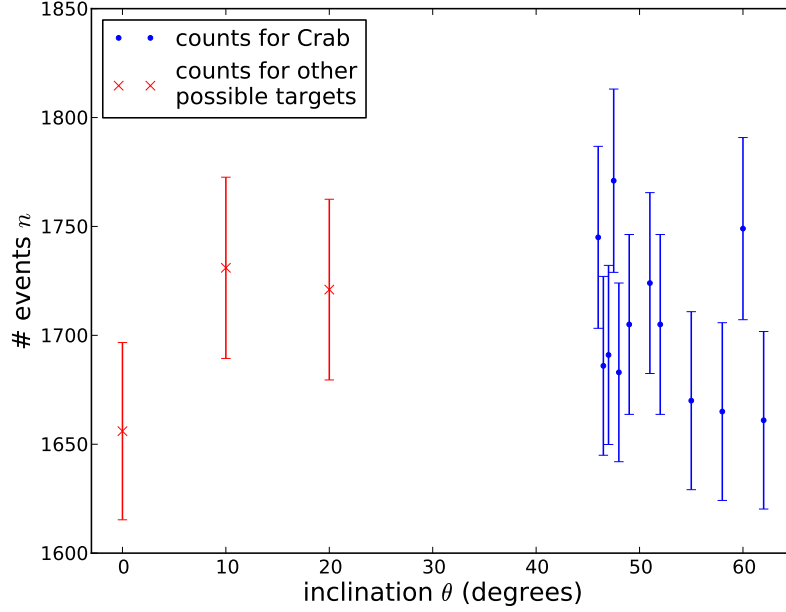


Figure 3.6: Simulated false event counts n from neuron background for various inclination angles θ . The blue dots correspond to the counts at inclination angles the Crab will be at during the pathfinder flight. The red x points correspond to inclination angles for targets closer to zenith that could be observed at some other time. Simulated observation time is half an hour at each angle.

between the two circle centres d . By looking again at figure 3.7a, we can see that the shaded region should have an area equal to a wedge cut out of each circle with angle 2ϕ minus the intersection of these wedges, the rhombus in the middle. The wedge has area A_w that is a fraction of the area of the circle A_s , based on the wedge's angle 2ϕ :

$$A_w = \frac{2\phi}{2\pi} \pi r^2 = \phi r^2, \quad (3.6)$$

and the rhombus where the wedges intersect has area hd , so

$$A_t = 2\phi r^2 - hd. \quad (3.7)$$

The angle ϕ can be computed based on d and r :

$$\phi = \arccos\left(\frac{d/2}{r}\right) = \arccos\left(\frac{d}{2r}\right), \quad (3.8)$$

and

$$h = r \sin(\phi). \quad (3.9)$$

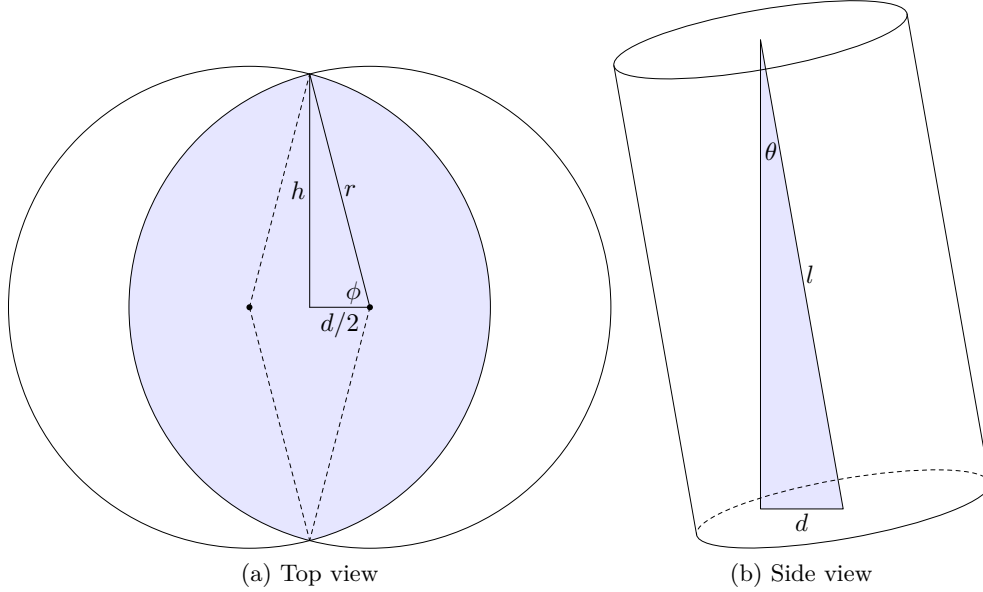


Figure 3.7: Area of a tilted slow scintillator that photons can still pass through. Scintillators in PoGOLite are hexagonal, but here they are approximated as cylinders for simplicity. The figure on the left shows a shaded area where photons can still pass through when the detector is tilted. Angle ϕ and length h are computed in (3.8, 3.9) and are used to calculate the area of this shaded region A_t in (3.7). The side view of the cylinder on the right shows how we can find the distance between the circles d ; see (3.10). r is the radius of the cylinder, l is its length, and θ is the inclination angle of the detector.

Now according to figure 3.7b we see that d can be computed based on the inclination angle θ and the length of the slow scintillator l :

$$d = l \sin \theta. \quad (3.10)$$

Now we can substitute (3.8), (3.9), and (3.10) into each other and (3.7) to get

$$A_t = 2 \arccos \left(\frac{l \sin \theta}{2r} \right) r^2 - r \sin \left(\arccos \left(\frac{l \sin \theta}{2r} \right) \right) l \sin \theta. \quad (3.11)$$

As mentioned in the beginning of this section, the area particles can pass through is proportional to the number of events, so $A_s \propto n_s$ and $A_t \propto n_t$ with the same proportionality constant. This means

$$\begin{aligned} \frac{n_t}{A_t} &= \frac{n_s}{A_s} \\ n_t &= \frac{n_s A_t}{A_s}. \end{aligned} \quad (3.12)$$

So, we can predict the number of events n_t for a inclination angle θ if we know an untilted event count n_s . A_t is given by (3.11) and A_s is just πr^2 , so

$$n_t = \frac{n_s}{\pi} \left(2 \arccos \left(\frac{l \sin \theta}{2r} \right) - \frac{1}{r} \sin \left(\arccos \left(\frac{l \sin \theta}{2r} \right) \right) l \sin \theta \right). \quad (3.13)$$

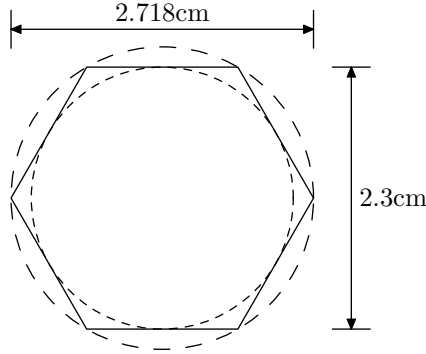


Figure 3.8: Interior dimensions of the slow scintillators. The dashed circles show the cross sections of the two cylinders used for calculation purposes to approximate the real hexagonal tube.

The length of the slow scintillator l is 60 cm, and the radius of our cylindrical approximation of the scintillator we take to be either 1.15 cm or 1.359 cm. These are half of the inner edge-to-edge and corner-to-corner width, respectively, of a hexagonal slow scintillator. Figure 3.8 shows the dimensions of the slow scintillator's cross section and how our two cylindrical approximations fit. The two circles act as minimum and maximum bounds for computing the area which particles can pass through.

Figure 3.9 shows curves with the predicted range of event counts based on a measurement $n_s = 7860$ events² per hour of observation with the detector pointed directly at its target, along with event counts from simulations using various small inclination angles. The simulated counts fit well with the predicted curves.

Table 3.2 shows the signal rates R_S (events per second) from the Crab for each of the inclination angles simulated and plotted in figure 3.9. Each R_S value is used to compute the minimum detectable polarization at the corresponding angle, using (3.3) with the other variables, $M_{100} = 0.278 \pm 0.005$, background rate $R_B = 0.947 \pm 0.007 \text{ s}^{-1}$, and observation time $T = 21,600 \text{ s}$, the same as in section 3.2. A 1° pointing error reduces R_S by half, from 2.18 ± 0.01 to 1.09 ± 0.02 per second, with a corresponding MDP increase from $8.52 \pm 0.19\%$ to $13.7 \pm 0.5\%$.

3.3.3 Potential hardware failure

A third potential problem that could detrimentally affect PoGOLite's observations are hardware failures. In this section the potential failure of a single PMT or

²This is one sixth of 47,160, the average number of events from 19 six-hour Crab simulations.

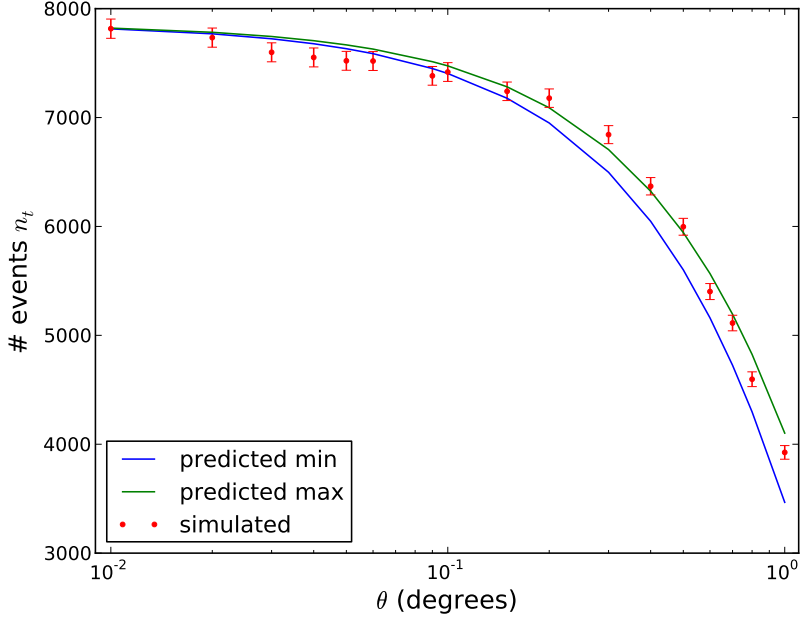


Figure 3.9: Number of events n_t for various small inclination angles θ from simulations of one hour observations, and curves showing the predicted range of counts computed with (3.13).

Table 3.2: Signal rates R_S of Crab events for various inclination angles θ from simulated one hour observations. R_S here has an uncertainty of $\pm 0.02 \text{ s}^{-1}$. MDPs are computed by extrapolating the given signal rate measured from a one hour simulation to the entire six hour observation. Background rate and M_{100} are the same as those used in section 3.2

θ (degree)	R_S (s^{-1})	MDP (%)	θ (degree)	R_S (s^{-1})	MDP (%)
0.01	2.17	8.54 ± 0.21	0.2	1.99	9.04 ± 0.24
0.02	2.15	8.59 ± 0.22	0.3	1.90	9.32 ± 0.25
0.03	2.11	8.70 ± 0.22	0.4	1.77	9.78 ± 0.26
0.04	2.10	8.73 ± 0.22	0.5	1.67	10.2 ± 0.3
0.05	2.09	8.76 ± 0.22	0.6	1.50	10.9 ± 0.3
0.06	2.09	8.76 ± 0.22	0.7	1.42	11.4 ± 0.3
0.09	2.05	8.87 ± 0.23	0.8	1.28	12.2 ± 0.4
0.1	2.06	8.84 ± 0.22	1.0	1.09	13.7 ± 0.5
0.15	2.01	8.98 ± 0.23			

an entire FADC (flash-analogue digital converter) board—the electronics which the PMTs are wired to—are considered.

PoGOLite has eight FADC boards wired to the PMTs in a pattern shown in figure 3.10. This “petal” pattern was chosen from a number of potential designs because it is expected to have the least impact on what is observed in the event of one of the FADC boards failing during the experiment [13].

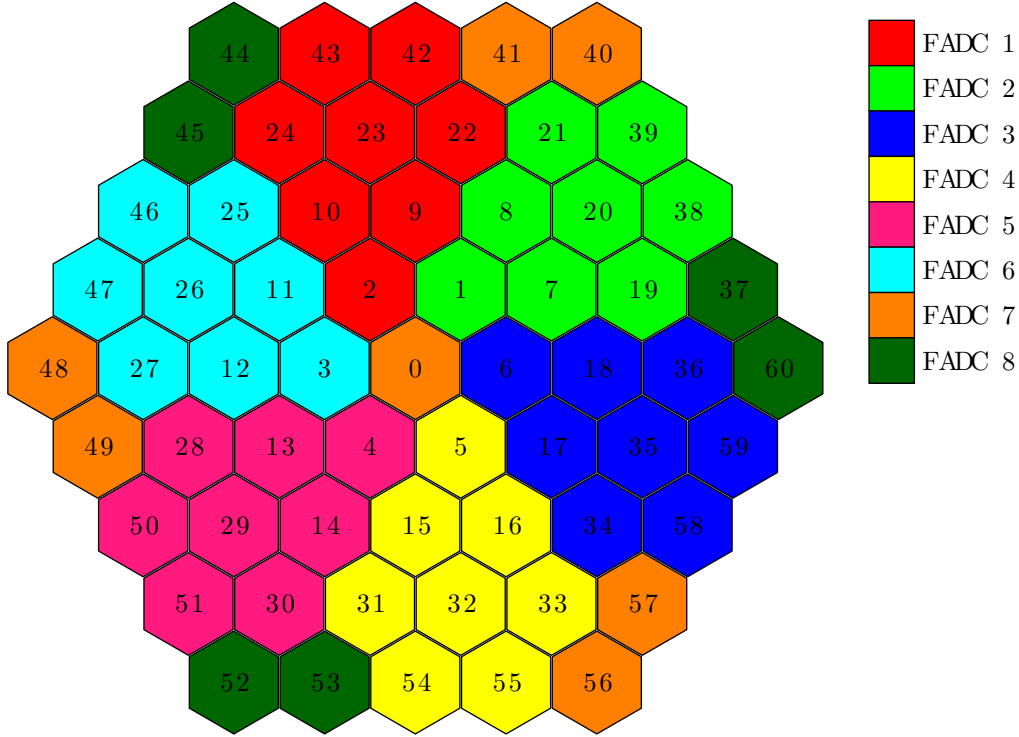


Figure 3.10: Arrangement of PDCs and their connections to FADCs.

FADCs 1-6 are all wired to the same pattern of PDCs, so only the failure of one of these will be considered. Additionally, the affects of FADC number 7 failing will be considered as it ought to be similar to losing FADC 8, only probably somewhat worse since it is wired to one more PDC. For the sake of testing the failure of just a single PMT, number 11 (named “Q-Bert”) was picked because this particular PMT has already shown some problems in pre-flight lab testing. Figure 3.11 shows the number of events measured for a six hour observation of a 100% polarized Crab source with the listed PMT or FADC considered unable to record any hits in corresponding fast scintillators.

Table 3.3 shows signal rates and the corresponding MDP computed with equation (3.3) for each of the PMT and FADC failures considered. For the sake of these computations the same M_{100} and background rate R_B are used as in previous sections. In reality, a lower background rate is likely to be observed along with the decreased signal rate when hardware has failed, but it could be difficult to simulate this accurately. A greater number of neutrons come from below (see section 2.2.4), so a PMT or group of PMTs that has failed on the side of PoGO facing down to-

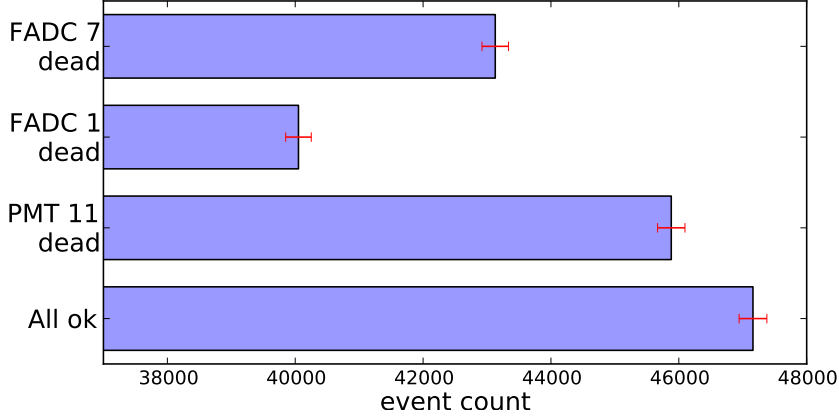


Figure 3.11: Number of events measured from a simulated six hour observation of a 100% polarized Crab source with some PMT or FADC hardware unable to record hits. Background triggered events are not included.

wards the earth could reduce the number of neutron-induced events significantly. However, during actual observations the entire polarimeter will be slowly rotated to avoid any kind of systematic bias such as this. Polaripogo is not currently capable of changing the rotation throughout a given simulation, so it would be necessary to combine several simulations with slightly different rotations in order to model this situation. Such a group of simulations will be left to future study, as it is beyond the scope of this thesis. In any case, the background event rate should not increase in the event of hardware failure, so using R_B from a simulations with all systems functioning should simply mean the MDP values calculated here are upper bounds.

Table 3.3: Crab signal rates R_S and MDP in the event of failures of PMTs or FADCs shown in figure 3.10. The signal is from a 100% polarized source, and MDP is computed based on $M_{100} = 0.278 \pm 0.005$, background rate $R_B = 0.947 \pm 0.007 \text{ s}^{-1}$, and observation time $T = 21,600 \text{ s}$.

Failed part	$R_S \text{ (s}^{-1}\text{)}$	MDP (%)
None	2.18 ± 0.01	8.52 ± 0.19
PMT 11	2.12 ± 0.01	8.67 ± 0.20
FADC 1	1.85 ± 0.01	9.49 ± 0.22
FADC 7	2.00 ± 0.01	9.01 ± 0.20

3.4 Polarization dataset

As was mentioned in chapter 2, observational data gathered during PoGOLite's flight will be compared with an array of data from simulations in order to determine

the polarization degree and angle of the photons coming from the Crab. This method is the same idea as used in [6] with observational data obtained by the INTEGRAL satellite. 19 polaripogo simulations were run, one with an unpolarized signal and the other 18 with a signal 100% polarized at $0^\circ, 10^\circ$, and every other tenth degree up to 170° . After extracting the valid events from the simulation output files in the manner described above in section 3.1, a Python program I wrote called `build_histogram_dataset.py` computes histograms of the distributions of scattering angles at each angle. By combining in appropriate proportions the bin counts of each of the polarized histograms with a histogram from the simulation of an unpolarized signal, a histogram for every degree of polarization from 0 to 100% is computed and saved.

Next, histograms for the intermediate angles $1^\circ, 2^\circ, \dots, 9^\circ$ and so on are computed by linearly interpolating between the existing histograms at angles that are multiples of 10° . This is done for each degree of polarization. Now a complete polarization dataset has been built with 18,180 entries representing every degree from 0-100% and angle 0- 179° .

Observational data can be compared with this dataset by binning the observed scattering angles into a histogram with the same bin boundaries as in the dataset, subtracting an appropriate number of background events, and computing the χ^2 test statistic between this histogram and each entry in the dataset. The polarization angle and degree corresponding to the lowest resulting χ^2 value is what we then estimate is the actual polarization of the measured signal.

Figure 3.12 shows an example of comparing a simulated signal polarized 46% at 123° with the polarization dataset. This is the polarization measured from the Crab by the INTEGRAL satellite [6]. No neutron background is considered in this case. The predicted polarization angle is $(124 \pm 2)^\circ$ and degree is $46_{-2}^{+3}\%$, which is a very close match to the actual signal.

Additional examples of fitting signals including background events and lower signal rates with the polarization dataset are discussed, along with more details about this analysis method, in [2].

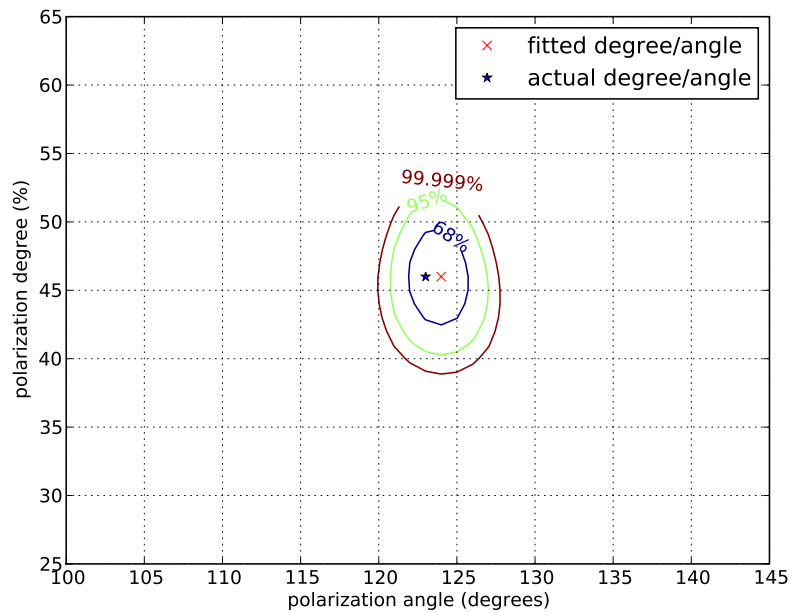


Figure 3.12: Finding the best fit of a simulated observation of a signal polarized 46% at 123° in the polarization dataset. Confidence levels around the fitted value are also shown, and the real degree and angle are within the 68% level.

Chapter 4

Conclusions and future work

I have made a number of enhancements to the polaripogo simulation software and scripts used for analysing its output data. It is now possible to specify the polarization angle of photons being fired at the simulated detector, the duration of an observation in terms of time instead of the number of particles to simulate, and the orientation of the simulated detector, all as convenient command line arguments. The process of finding all valid events from a simulation output file, with their azimuth scattering angle and deposited energies, has been reduced to a one step process from the three separate scripts that had to be run previously [19].

Using the improved simulation and analysis software, I have studied how a few potential problems affect the data gathered:

- Changes to the inclination angle of PoGOLite as it tracks its target(s) across the sky are unlikely to have a significant impact on the effects of neutron background.
- Errors in the detector's aim at its target affected simulated results in close to the same way as predicted by calculations based on PoGOLite's geometry. A 1° pointing error reduces the rate of observed events from the Crab from 2.18 ± 0.01 to 1.09 ± 0.02 per second, increasing the MDP for a six hour observation from $8.52 \pm 0.19\%$ to $13.7 \pm 0.5\%$.
- Loss of a single PMT reduces the Crab signal rate to 2.12 ± 0.01 events per second from 2.18 ± 0.01 , or if an entire FADC fails the signal rate is reduced to as low as 1.85 ± 0.01 per second. The MDP for a six hour observation at these rates is $8.67 \pm 0.20\%$ and $9.49 \pm 0.22\%$, respectively, for the loss of the PMT or FADC.

Together with Cecilia Marini Bettolo [2] I also wrote new code for building up a polarization dataset and using it to find the polarization angle and degree of simulated photons from an unknown source. This method is expected to be valuable when analysing real data obtained from upcoming PoGOLite flights.

4.1 Future work

One additional study that I considered undertaking was to see what affect rotating PoGOLite during its simulated observations might have on measurements. Perhaps this could help find systematic bias in the detector's design. Also, it would be helpful in determining how neutron background effects might change in the event of a failure of FADC or PMT hardware, as mentioned in section 3.3.3.

Also related to hardware failure, the effect of a failure of an FADC board or PMT connected to the side anti-coincidence shields would be interesting to examine. With one or more SAS detectors inoperable, background induced events would certainly increase, and potentially have a significant impact on results.

Finally, it would be interesting to try changing the output file format used by polaripogo. Currently it prints its output data in an ascii text file. For relatively long simulations, this file can become very large, especially when simulating neutron background. While working on this thesis I often encountered ran out of disk space due to the size of these files. It is possible that disk usage could be reduced by writing data out instead to a structured binary file format, using a software tool such as Protocol Buffers¹. This would remove the need to have text labels identifying data field repeated millions of times, and reading from the file would not require the complicated string parsing that our current analysis does. Furthermore, polaripogo output files store numerical values now with only a few digits of accuracy. When written in binary format, floating point numbers take up only a four or eight bytes while providing eight or 16 digits of accuracy, respectively.

¹<http://code.google.com/p/protobuf/>

Appendix A

Using polaripogo software

Polaripogo can be obtained from its Subversion [21] repository using the following command on a Unix-like system:

```
$ svn co svn://pogosim.particle.kth.se/polaripogo/trunk ./polaripogo
```

Contact Mark Pearce for access to the repository (contact information available at <http://www.particle.kth.se/~pearce/>).

Instructions in the following sections can also be found in the `Readme` file included with the source code. Please note that this `Readme` may be more up to date than the information here.

A.1 Building

Polaripogo requires Geant4, GNU make, and a C++ compiler. Note that, as of Geant4 9.2.p01, there are problems with the implementations of Rayleigh and Compton scattering in Geant4 [10]. This can be worked around by patching Geant4 with `patches/geant4_polar.diff`. Apply the patch according to the instructions in the `.diff` file, then compile Geant4 as normal.

Once Geant4 is installed, be sure to set the environmental variables it needs. Geant4 provides scripts to do this, `bin/env.sh` and `bin/env.csh`, in the directory which Geant4 has been installed to (e.g. `/usr/local/geant4`).

Now you can compile polaripogo with the `make` or `gmake` command (depending on your system). The compiled program is `$G4WORKDIR/bin/$G4SYSTEM/polariPoGO`. You can remove the compiled binaries using `make clean` or `gmake clean`.

A.2 Running simulations

Run `polariPoGO` without any arguments to see a summary of available options. You will need to at least supply the `-m` argument to give a macro file containing simulation parameters. See `run.mac` for an example, or `vis.mac` for some parameters

used when visualizing the detector. Additionally, the `-t` argument is required to give the length of the observation (in seconds) if one is not using visualization.

As an example, the following command would should be used to simulate one hour of neutrons with the detector at a 30 degree inclination angle from zenith. Here `/crgen/model` should be `CrNeutron` in `run.mac`. Note that `-h` is given; this option should be used when modelling neutrons:

```
$ polariPoGO -m run.mac -t 3600 -h -i 45
```

Next, this command starts a simulation of 30 minutes with the detector pointed directly at the Crab (`/crgen/model CrCrab` in `run.mac`). The photons simulated are 100% polarized at 60 degrees, and the Geant4 random number is seeded at 875. This seed should be changed for each simulation, and if unspecified Geant4 will use the same default every time:

```
$ polariPoGO -m run.mac -t 1800 -a 60 -s 875
```

The output of a simulation will be in a file named according to the model used and the `a`, `d`, `i`, `r`, `s`, and `t` options, with a `.dat` file extension. For instance, the first command above would create an output file `neutron_t=3600_i=45.dat` and the second would create `crab_a=60_t=1800_s=875.dat`. Additionally, the files `PDCpos.dat`, `SASpos.dat`, `CrGenModel.dat`, and `Geometry.dat` are created to store detector geometry and cosmic-ray model information.

A.3 Analysis

The `script/` directory contains numerous Python [23] and ROOT [3] scripts that can be used for analysing the `.dat` files generated by simulations. Note that the Python scripts have only been tested with Python 2.6 and may use some language features not available in earlier releases.

- `extract_events.py`: Reads in the output file from a polaripogo simulation and finds those events that will be counted as hits by the simulated detector. Each valid hit will be saved to an output file with the azimuth scattering angle and deposited energy.
- `histogram_from_events.py`: Plots histograms of the scattering angle and signal rate for the energy range 25-80 keV based on one or more events files generated by `extract_events.py`.
- `build_histogram_dataset.py`: Reads in events files generated from several simulations of polarized Crab sources and an unpolarized one, then combines these to build histograms of the scattering angles for all possible polarization angles from 0-179 degrees and degree 0-100%. These are saved in a Python dictionary and written to a file that can be used by other scripts below. The event file names must be put into this script itself before running.

- `histogram_from_dataset.py`: Plots the scattering angle histogram for a given polarization degree and angle from the dataset created by the previous script.
- `find_polarization.py`: Given a histogram of scattering angles, finds the closest matching degree and angle from the dataset using a Chi-square test.
- `dig_mod_analysis.py`: Extracts data from a polaripogo simulation and saves it in a format that the older Root scripts (below) expect to read in.
- `ModulationAnalysis_airAtten.cc` and `ModulationAnalysis_combined.cc`: These plot a number of histograms from a `.mod` file (which is produced by `dig_mod_analysis.py`) showing scattering angle, energy distributions across scintillators, and so on. These scripts generally need to be modified according to simulation parameters and the name of the `.mod` file to read, so please read through them carefully if you wish to use them.

The comments at the top of these scripts provide more information about what they do and how they are used.

A.4 History

Polaripogo was originally written for simulations of the full 217 detector PoGOLite by Tsunefumi Mizuno with parts derived from GLAST and LAT simulations. This code was modified and extended by Kristoffer Myrsten for the 61 detector PoGOLite pathfinder instrument and for optimizing the design of the neutron shield [19].

I set up the Subversion repository mentioned above to track changes to the source code and facilitate easier collaborative development. I then merged in some recent changes Mizuno had made on his original branch of the code [17]. The work from Myrsten had not been integrated back with this original branch, and Mizuno had done additional work on the original code base after the version that Myrsten started with. Details of this merging process and the additional modifications made to the software discussed throughout this thesis can be found by inspecting the subversion repository history and logs.

List of Figures

1.1	Crab Nebula viewed from the Hubble Space Telescope	2
1.2	Components of the PoGOLite polarimeter	4
1.3	Valid and background events measured by PoGOLite	5
2.1	PoGOLite as rendered by the polaripogo simulation software	8
2.2	Arrangement of detector and photon trajectories for Crab simulations .	11
2.3	Coordinate system for picking direction of incoming particles	13
2.4	Inclination angles for direction of incoming neutrons	14
3.1	Uncertainty of azimuth angle	17
3.2	Effect of smearing azimuth angles on modulation	18
3.3	Distribution of number of events repeatedly measured from a simulation	19
3.4	Scattering angle distributions from six hour simulations	20
3.5	Elevation angle of targets during pathfinder flight	22
3.6	Simulated false events from background at various inclination angles . .	23
3.7	Area of a tilted slow scintillator that photons can still pass through . .	24
3.8	Interior dimensions of the slow scintillators	25
3.9	Event counts for various small pointing errors	26
3.10	Arrangement of PDCs and connections to FADCs	27
3.11	Number of events measured from Crab with hardware failures	28
3.12	Finding best fit within the polarization dataset of simulated observation	30

List of Tables

3.1	Quenching in fast and slow scintillators	16
3.2	Signal rates and MDP for various small pointing errors	26
3.3	Crab signal rates and MDP in the event of hardware failures	28

Bibliography

- [1] T. W. Armstrong, K. C. Chandler, and J. Barish. Calculations of Neutron Flux Spectra Induced in the Earth's Atmosphere by Galactic Cosmic Rays. *Journal of Geophysical Research*, 78(16):2715–2726, 1973. ISSN 0148–0227. DOI: 10.1029/JA078i016p02715.
- [2] C. Marini Bettolo. *Performance Studies and Star Tracking for PoGOLite*. PhD thesis, Kungliga Tekniska högskolan. In preparation.
- [3] R. Brun and F. Rademakers. ROOT – An Object Oriented Data Analysis Framework. In *Proceedings AIHENP'96 Workshop*, Lausanne, September 1996. <http://root.cern.ch/>.
- [4] B. W. Carroll and D. A. Ostlie. *An Introduction to Modern Astrophysics*. Addison-Wesley, second edition, 2007. ISBN 0321442849.
- [5] O. Engdegård. Studies of Energy Dependent X-Ray Polarisation with PoGO-Lite – Monte Carlo Simulations with Geant4. Master's thesis, Kungliga Tekniska högskolan, 2006.
- [6] A. J. Dean et al. Polarized Gamma-Ray Emission from the Crab. *Science*, 321(5893):1183–1185, 2008. ISSN 1095–9203. DOI: 10.1126/science.1149056.
- [7] M. Axelsson et al. Measuring energy dependent polarization in soft [gamma]-rays using Compton scattering in PoGOLite. *Astroparticle Physics*, 28(3):327–337, 2007. ISSN 0927–6505. DOI: 10.1016/j.astropartphys.2007.06.006.
- [8] S. Agostinelli et al. Geant4 – A Simulation Toolkit. *Nuclear Instruments and Methods A*, 506:250–303, 2003. <http://geant4.cern.ch/>.
- [9] T. Kamae et al. PoGOLite – A High Sensitivity Balloon-Borne Soft Gamma-ray Polarimeter. *Astroparticle Physics*, 30(2):72–84, 2008. ISSN 0927–6505. DOI: 10.1016/j.astropartphys.2008.07.004.
- [10] T. Mizuno et al. Beam test of a prototype detector array for the PoGO astronomical hard X-ray/soft gamma-ray polarimeter. *Nuclear Instruments and Methods A*, 540(1):158–168, 2005. ISSN 0168–9002. DOI: 10.1016/j.nima.2004.11.009.

- [11] V. V. Verbinski et al. Calibration of an organic scintillator for neutron spectrometry. *Nuclear Instruments and Methods*, 65(1):8–25, October 1968. DOI: 10.1016/0029-554X(68)90003-7.
- [12] R. Feynman, R. Leighton, and M. Sands. *The Feynman Lectures on Physics*, volume 1. Addison-Wesley, 1963.
- [13] M. Jackson. Notes on the PMT mapping scheme. PoGOLite collaboration internal document, June 2009.
- [14] J. Kazejev. Studies of Neutron Backgrounds for PoGOLite – a Balloon-borne Gamma-ray Polarimeter. Master’s thesis, Kungliga Tekniska högskolan, 2007.
- [15] M. Kiss. Studies of PoGOLite Performance and Background Rejection Capabilities. Licentiate thesis, Kungliga Tekniska högskolan, 2008. ISBN 978–91–7415–029–2.
- [16] L. Lönnblad. CLHEP - a Project for Designing a C++ Class Library for High Energy Physics, 1994. <http://proj-clhep.web.cern.ch/proj-clhep/>.
- [17] T. Mizuno. Private communication, July 2009.
- [18] T. Mizuno. Private communication, 2009.
- [19] K. Myrsten. Polarised Gammay-ray Observer (PoGOLite) Pathfinder Experiment: Neutron Shield Design and Limits on Polarisation Measurements. Master’s thesis, Kungliga Tekniska högskolan, 2008.
- [20] M. Pearce. Observation targets – 2010. PoGOLite collaboration internal document, September 2009.
- [21] C. Pilato, B. Collins-Sussman, and B. Fitzpatrick. *Version Control with Subversion*. O’Reilly Media, Inc., 2008. ISBN 9780596510336. <http://subversion.apache.org/>.
- [22] J. A. Simpson. Neutrons Produced in the Atmosphere by the Cosmic Radiations. *Physical Review*, 83(6):1175–1188, September 1951. DOI: 10.1103/PhysRev.83.1175.
- [23] G. van Rossum. Python reference manual. Technical report, Amsterdam, The Netherlands, 1995. <http://www.python.org/>.
- [24] E. W. Weisstein. Sphere Point Picking. MathWorld – A Wolfram Web Resource. <http://mathworld.wolfram.com/SpherePointPicking.html>. Accessed 2009-11-25.